RSC Advances

PAPER

View Article Online
View Journal | View Issue

Cite this: *RSC Adv.*, 2017, **7**, 38647

Design of a multifunctional vanadium pentoxide/polymer biocomposite for implant-coating applications†

N. Anicic, *[ab] M. Vukomanovic[a] and D. Suvorov[a]

In this study we designed a multifunctional implant coating by exploiting the properties of vanadium pentoxide (V_2O_5), *i.e.*, the antibacterial activity *via* myeloperoxidase-like catalytic activity and the bioactivity of low concentrations of vanadate ions (dissolved form of V_2O_5) *via* the insulin-mimicking effect. To achieve this, the dissolution control of the V_2O_5 and the sustained release of the vanadate ions had to be achieved by processing the appropriate carrier system for the V_2O_5. Thus, we evaluated the ability of different polymeric carriers and the V_2O_5 particle morphology to modulate *in vitro* the stability of the prepared V_2O_5/polymeric coatings. For the control of the V_2O_5 dissolution it was crucial to control the diffusion of the particles from the polymeric matrix to the surrounding medium and to prevent extensive swelling of the polymer matrix. We highlighted the correlation between the strength of the interactions at the V_2O_5/polymer interface and the composite's stability under simulated physiological conditions. The optimum outcome was obtained for a nanowires-V_2O_5/PLGA composite coating that delivered vanadates sustainably, while at the same time preventing the colonization of *S. epidermidis* (NCIMB 8853) on its surface and ensuring the absence of any harmful effects on the red blood cells.

Received 9th June 2017
Accepted 23rd July 2017

DOI: 10.1039/c7ra06471c

rsc.li/rsc-advances

Introduction

If effectively stabilized, vanadium pentoxide (V_2O_5) is a potential multifunctional material that exhibits antibacterial and bioactive properties. This material could be used for implant coatings, as it could successfully target the "race for the implant surface" between cells and bacteria.[1] Recent studies have highlighted the ability of nanostructured V_2O_5 to mimic the myeloperoxidase activity,[2,3] which is effectively utilized for the processing of an anti-biofouling ship-hull coating.[3] Myeloperoxidase is an enzyme that is present in human neutrophils. Its role is to eliminate bacteria *via* catalysis of the hydrogen-peroxide-to-hypochlorite transformation in the presence of chloride ions.[4] In this context there is a possibility to exploit the unique property of V_2O_5 to design antimicrobial coatings for applications in medicine, which has so far not been discussed.

The use of V_2O_5 in medicine is limited by its relatively high solubility in aqueous media (>1 g l^{-1}), while the so-formed, high concentrations of vanadate ions are toxic to human cells.[5,6] However, *in vitro* studies also showed their bi-phasic nature, as these ions are able to stimulate the cell proliferations of various types of mammalian cells at low concentrations (up to 10 μM).[7,8] They exhibit an insulin-mimicking action *via* the inhibition of tyrosine phosphatase.[9] *In vivo* studies of rats proved that orally administrated vanadates stimulated the orientation of the fibroblasts in parallel arrays early in the tissue-repair process, *i.e.*, vanadate ions can accelerate tissue repair.[10–12] Further studies confirmed that vanadates improved the bone-formation rate, the mechanical strength and the mineralization,[13] while the pro-oxidant potential of vanadates was not revealed in erythrocytes.[14] These studies confirmed the bioactive potential of the vanadate ions when they are properly delivered.

V_2O_5 could be used as a source of vanadate ions if its solubility is strictly controlled. To do this, V_2O_5 has to be integrated inside a composite. Polymers are widely used as carriers for the controlled administration of molecules, macromolecular species or nanoparticles.[15–17] Some of them, including poly (lactic-co-glycolic) acid (PLGA), polylactic acid (PLA), polystyrene (PS) and chitosan, are already established as very effective drug-delivery systems. These polymers differ in their properties (including their hydrophilic/hydrophobic character, the rate and extent of their biodegradability, surface chemistry, *etc.*), which can be effectively used to design a drug-delivery system in line with the requirements of the final application, *i.e.*, to retain the catalytic activity of the V_2O_5 and keep the level of eluted vanadates below 10 μM. The controlled release of active substances from these systems is a complex process that

[a]*Advanced Materials Department, Jozef Stefan Institute, Jamova Cesta 39, SI-1000 Ljubljana, Slovenia. E-mail: nemanja.anicic@ijs.si*

[b]*Jozef Stefan International Postgraduate School, Jamova Cesta 39, SI-1000 Ljubljana, Slovenia*

† Electronic supplementary information (ESI) available. See DOI: 10.1039/c7ra06471c

is influenced by the physico-chemical properties of the polymer matrix, the release medium and the active compound (V_2O_5). In general, the diffusion of the active material, the polymeric matrix swelling and the matrix degradation are considered to be the main driving forces for the elution of the drug from the matrix.[18] One of the common outcomes is a burst release of the active species from the matrix during the first few hours of exposure.[16,19] Such an outcome has to be avoided for V_2O_5/polymer biocomposites, which makes the stabilization of V_2O_5 within the polymer matrix critical during the initial stage of the exposure to aqueous media.

We were processing an innovative multifunctional V_2O_5/polymer composite system in the form of a coating that is capable of retaining the antibacterial properties of V_2O_5 and, at the same time, providing strict control over the vanadate-release kinetics during the initial stage of its exposure to the medium. For this purpose, we evaluated and explained the impact of the V_2O_5 particle morphology and the interface interactions on the *in vitro* performance of V_2O_5/polymer composite coatings.

Materials and methods

Synthesis and processing methods

Synthesis of V_2O_5. The 1D nanostructured V_2O_5 was synthetized using a hydrothermal method.[20] Commercial V_2O_5 powder (99% purity, purchased from Alpha Aesar) was dissolved in 50 ml of H_2O_2(aq). The final vanadium concentration was 0.06 M and the molar ratio V : H_2O_2 was 1 : 10. The as-prepared solution was transferred to a Teflon-lined autoclave, sealed and held at 200 °C for 24 h. At the end of the process the precipitate was collected, washed with deionized water and lyophilized.

Preparation of V_2O_5/polymer composite coatings. A solvent-casting method was used to prepare the composite coatings. The total mass of the composite coatings was set to 60 mg. The solution of PLGA (monomer ratio 50 : 50, Resomer RG 505, Evonik Industries) in dichloromethane (40 mg ml^{-1}) was mixed with 1.5 ml of a suspension of V_2O_5 (varied from 0.08 to 4 mg ml^{-1}) in dichloromethane and left under the hood overnight to allow for the solvent's evaporation. The embedding of V_2O_5 NWs in a PLA (Resomer LR 704 S, Evonik industries) or PS (99% purity, Sigma Aldrich) matrix involved the same procedure as with PLGA. Chitosan (purity 99%, Sigma Aldrich) was dissolved in 1% acetic acid solution instead of dichloromethane during the V_2O_5/chitosan composite coating's preparation procedure.

Methods of physico-chemical characterization

X-ray diffraction analysis (XRD). The phase composition of the hydrothermally prepared inorganic material was analysed using a Bruker AXS D4 Endeavor X-ray diffractometer in the angular range from 5° to 70° with a 3 s step of 0.02°. For this purpose, as-prepared materials (without previous crushing in a mortar) were placed on the XRD holder and sealed with Kapton foil.

Scanning and transmission electron microscopy (SEM and TEM). The examination of the morphology for the V_2O_5 particles and the composite surface was performed using SEM analysis (JEOL JSM 7600F). The particles were dispersed in ethanol and dried on an Au-sputtered, 100 nm polycarbonate filter membrane. The membrane was fixed on the carbon tape and coated with approximately 5 nm of carbon. The V_2O_5/polymer composites were stuck on the carbon tape and carbon coated before observation. High-resolution TEM and selected-area diffraction (SAED) analyses were performed on a JEOL JSM 2100 with a LaB_6 electron source. Before the observation the V_2O_5 particles were ultrasonically dispersed in ethanol. The as-prepared suspension was dripped onto a Cu TEM grid covered with lacy carbon.

Specific-surface-area analysis. The specific surface areas of the V_2O_5 powders were determined with the Brunauer–Emmett–Teller (BET) method using a Micromeritics Gemini II 2370 nitrogen-adsorption apparatus (Norcross, GA).

Fourier-transform infrared spectroscopy (FTIR). FT-IR analyses were conducted on a Perkin Elmer Spectrum 400 MIR spectrophotometer using the attenuated total-reflection (ATR) technique. The obtained data was used to provide information about the intermolecular interactions at the interface between the polymer chains and the V_2O_5 particles. The mass ratio between the polymer and the particles in the composites was 1 : 1. The ATR-IR spectra were obtained in the range 650 to 4000 cm^{-1}.

In vitro vanadate elution kinetics

Dissolution of V_2O_5. To determine the solubility kinetics of the pure V_2O_5 particles, 5 mg of material was placed in 10 ml of phosphorus buffered solution (PBS) at 37 °C and linearly shaken at a rate of 60 rpm. The 500 μL aliquots of prepared suspensions were taken at regular time intervals and centrifuged in a MPW-55 micro-centrifuge at 14 500 rpm for 15 min to obtain clear, particle-free supernatants that were removed and stored for a later quantification of the vanadate ions. The measurements were performed in triplicate.

Release of the vanadate ions from the composites. The elution kinetics of the vanadate ions from the V_2O_5/polymer composites was determined when 60 mg of the composite was exposed to 20 ml of PBS at 37 °C and shaken at a rate of 60 rpm. The 500 μL aliquots from body fluid were taken at regular intervals and stored for subsequent quantification of the released vanadates. The changes in the volume of body fluid were took into account and a recalculation of the measured vanadates' concentration values was performed. After the exposure, the composites were washed, dried and stored for SEM observations of their surfaces. The measurements were performed in triplicate. The drying of the composites containing PLGA and PLA was under ambient conditions, while the chitosan-based composites were fast frozen in liquid nitrogen and lyophilized to avoid structural modifications during drying.

Quantification of the released vanadate ions. The concentrations of the vanadate ions released during the elution-kinetics studies were determined spectro-photometrically using 4-(2-pyridylazo)-resorcinol (PAR) and hydrogen peroxide.[21] A total of 400 μL of 2.5×10^{-5} PAR solution was mixed with 100 μL of a supernatant solution, 100 μL of 1 M

H_2SO_4 and 100 μL of 3% H_2O_2 (w/w) water solution in a 1 ml volumetric flask that was filled to the label with deionized water. The as-prepared solution was kept for 2 h at room temperature and the absorbance was measured at 542 nm using a Shimadzu UV-3600 spectrophotometer. Standard solutions for a calibration curve were prepared for the concentration range from 0.025 mg l^{-1} to 3 mg l^{-1} using NH_4VO_3 (99.9%, Sigma Aldrich).

Antibacterial activity studies

Live/dead viability test of planktonic bacteria. We used a precise live/dead assay kit (L70007 BacLight, Molecular Probes) to monitor the viability of the bacteria when exposed to V_2O_5. The test was performed according to the user manuals. Briefly, the ratio between the green- and red-light fluorescence is a linear function of the percentage of live bacteria, so the portion of the live bacteria in a specific mixture was determined using the calibration curve. To obtain the calibration curves, the fluorescence ratios were determined from suspensions with known viability. The 2 ml of bacteria (10^6 CFU ml^{-1}) in the phosphate buffer were exposed for 3 h to V_2O_5 at 0.2 mg ml^{-1}, 0.1 M of chloride ions and to 10 μM of hydrogen peroxide. The viability of the bacteria in the control solutions was also assessed. The measurements were performed in four replicates. After 3 h, the suspensions were centrifuged at 2000*g* for 10 minutes and the supernatant was poured out. Two hundred μL of fresh phosphate buffer was added, the pellet was resuspended and then mixed with the kit components. After 15 minutes of incubation, the ratios between the green- and red-light fluorescence were determined in the microplate reader and the percentages of the live bacteria were calculated from the measured calibration curves. The activity of the V_2O_5 was evaluated against *E. coli* (strain MG1655, ATCC 47076) and *S. epidermidis* (NCIMB 8853).

Crystal violet assay for testing bacteria colonization. The *S. epidermidis* colonization of the coatings' surfaces was assessed with a crystal violet (CV) assay. The coatings were prepared inside 20 ml vials so that the concentration of V_2O_5 was 0.1 mg cm^{-2}. Some 107 CFU cm^{-2} of bacteria in a sterile physiological solution were transferred to vials and incubated for 24 h. The measurements were performed in five replicates. The physiological solution was enriched with glucose, which led to biofilm formation on the coatings' surfaces instead of its formation at the liquid/air interface. After incubation, the coatings were washed with PBS and carefully removed from the vials. The crystal violet absorptions, extraction and absorbance measurements were made as explained in literature.[22]

Evaluation of the strength of bacteria/coating interactions. The bacteria colonization of the coating's surfaces was performed as previously described. The suspension of bacteria above the coating was vigorously mixed with a pipette and smeared on the agar plates. These plates were transferred to an incubator at 37 °C and incubated for 24 h to evaluate the colony growth. The measurements were performed in five replicates.

Live/dead test for detecting the viability of colonized bacteria. The BacLight makes it possible to observe the bacteria using fluorescence microscopy. The bacteria colonization of the coating's surfaces was performed as previously described. After rinsing with the PBS, the coatings were removed from the wells and the kit solution was added. The added volume was proportional to the measured CV absorbance. The coatings were then on an objective glass, covered with a cover glass and observed under the microscope with green and red fluorescent filters (Eclipse Ti-U inverted microscope, Nikon). The incubation time was fixed at 15 minutes.

Hemocompatibility studies

Determination of percentage of hemolyzed cells. Fresh whole sheep blood by the Veterinary Faculty, University of Ljubljana from their sheep flock as part of regular serological monitoring program. The withdrawal of the blood was performed by using BD Vacutainer® blood collection kit and was transferred to tubes with additionally added Alsever's medium to be used within the 7 days as a source of red blood cells (RBCs). The Alsever's medium contained 4.2 g l^{-1} of NaCl (Carlo Erba Chemicals, 99%), 2.17 g l^{-1} of sodium citrate dihydrate (Sigma Aldrich, 99.8%) and 20 g l^{-1} of D-glucose (Sigma Aldrich, 99.5%). The experiments on the RBCs were performed in accordance with the national regulations (št. 003-02-5/2011-26) and biosafety guidelines implemented at Jožef Stefan Institute.

Before use the red blood cells were diluted in the HEPES buffer (Sigma Aldrich, 99.5%) to a final concentration of 5×10^7 RBC per ml. The RBCs were incubated with the prepared materials for 24 h. After the exposure, the cells were centrifuged at 1000*g* for 10 minutes. The supernatants were evaluated for haemoglobin content by the means of UV/Vis absorption at 415 nm (Synergy H1, Biotec).

Morphology of RBCs. After the exposure to the V_2O_5 nanowires, the red blood cells were collected on the polycarbonate membrane, washed in physiological solution three times and incubated for 30 min in 2% glutaraldehyde solution (Sigma Aldrich). After the incubation, the membrane was washed in deionized water three times and lyophilized. Before the SEM observation, the membrane containing RBCs was fixed on the carbon tape and coated with 5 nm of platinum. The same preparation procedure was applied for the coatings in contact with the RBC. The coatings were washed gently, to avoid excessive detachment of the RBCs from the surface.

Statistical analysis. The average values and sample standard deviations were calculated. Each sample population (4 replicates) was tested for the existence of outliers. We used a two-sided *t*-test for independent samples to assess the differences between the two sample averages.

Results

Morphology and structure of V_2O_5 powders

Before embedding inside the composites, we made a structural characterization of both the commercial and the hydrothermally prepared V_2O_5 powders. In both cases the XRD patterns matched the orthorhombic crystal structure of the V_2O_5 (JCPDS card 85-0601) and exhibited the same phase composition (Fig. 1a). In comparison to the commercial V_2O_5, the diffraction

pattern of the hydrothermally prepared V_2O_5 exhibited only (0*kl*) peaks, *i.e.*, the diffraction peaks representing the (110), (101), (111), (130), (121), (141) and (102) crystallographic directions were not observed (Fig. 1a). These findings indicate that the hydrothermally prepared V_2O_5 crystals displayed a preferential orientation, which was not the case for the crystals of the commercial powder.

The difference in the orientation of the hydrothermally prepared and commercial V_2O_5 particles was further studied using SEM analyses. The average size of the commercial V_2O_5 crystals was 230 ± 25 nm. These crystals had an irregular shape, a low aspect ratio and did not show any preferential orientation (Fig. 1b), so they were denoted as 0D V_2O_5 sub-microparticles (V_2O_5 MPs). In contrast, the hydrothermally prepared V_2O_5 crystals exhibited a significant anisotropy and a high aspect ratio, characteristic for a 1D nanowire morphology and were denoted as V_2O_5 NWs (Fig. 1c). The average width of the particles was 40 ± 10 nm, while the average length was 26 ± 15 μm. Each individual nanowire was a single crystal, as point diffraction was observed in the SAED pattern (Fig. 1d). These crystals possessed a highly ordered crystal structure and a very thin amorphous layer (less than 0.5 nm) at the surface (Fig. 1d, white dashed triangle). The interplanar distances in both the SAED and the HR-TEM were complementary and confirmed the preferential growth of the nanowires along the [100] direction.

The difference in the morphology caused a significant difference in the BET surface areas of the commercial and hydrothermally prepared V_2O_5. The commercial V_2O_5 MPs had a specific surface area of 4.5 $m^2\ g^{-1}$, while the specific surface area of the prepared V_2O_5 NWs was 30.7 $m^2\ g^{-1}$. The anisotropy and the larger specific surface area of the 1D nanowires were expected to allow easier processing and obtaining a higher level of homogeneity for the V_2O_5/polymer composites.

The role of particle morphology on the solubility control of V_2O_5

The solubility assay showed that the initial rate of dissolution was higher for the V_2O_5 NWs than for the commercial V_2O_5 MPs in the PBS medium (Fig. 2a). The vanadates' concentration in the V_2O_5 nanowire suspension was almost four times higher than the corresponding concentration in the commercial V_2O_5 suspension after 6 h of exposure. The levels of the vanadates were equalized in both suspensions after a long exposure ($t = 8$ days) to the PBS medium. Thus, there is a difference in the kinetics of dissolution, which is faster for the 1D nanoparticles than for the 0D sub-micron particles. There was no difference observed in the thermodynamics of the dissolution. The nanoparticles dissolved faster than the microparticles[6] due to the larger surface available for an interaction with the solvent (30.7 *vs.* 4.5 $m^2\ g^{-1}$ in our study).

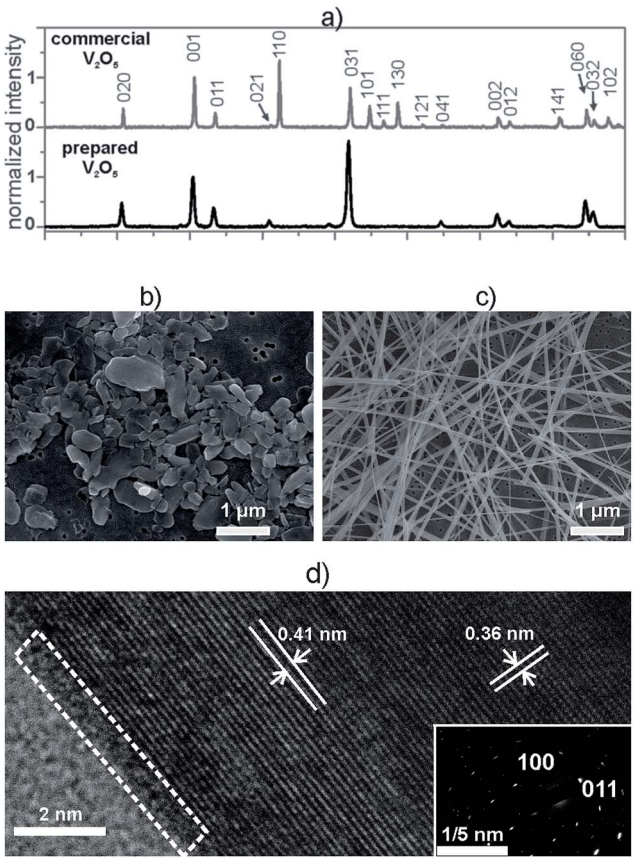

Fig. 1 (a) Powder XRD patterns. All intensities are normalized against the intensity of the (001) diffraction; morphology of (b) the commercial V_2O_5 particles and (c) the prepared V_2O_5 particles; (d) HR-TEM and SAED study of an individual particle of prepared V_2O_5.

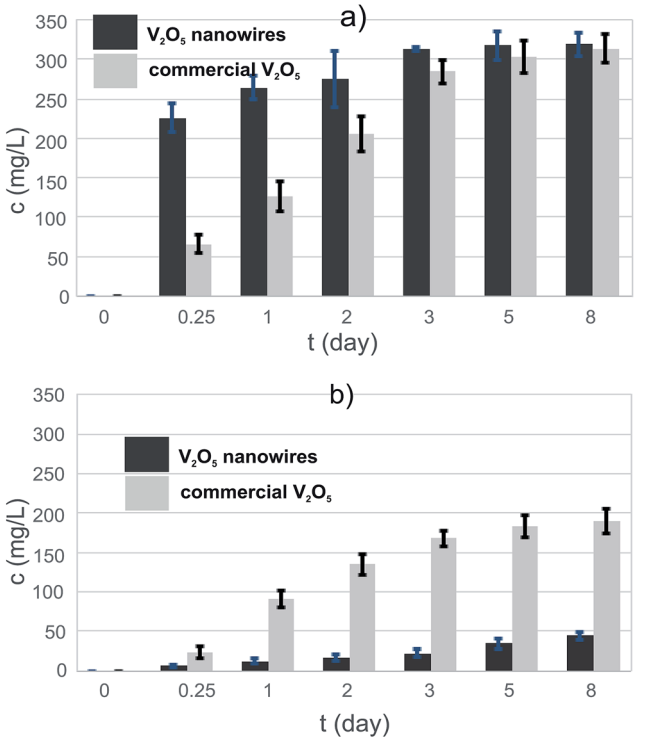

Fig. 2 The increase of vanadate concentration after exposure to PBS medium of (a) pure V_2O_5s and (b) V_2O_5/PLGA composites.

The level of the eluted vanadates in both V_2O_5 suspensions was two orders of magnitude above the bioactivity concentration range,[7] which confirmed the need for an efficient vanadate-delivery system. Thus, the ability of the PLGA to reduce the dissolution of V_2O_5 in the PBS was tested for both powders. The PLGA matrix was able to reduce the vanadate elution to the PBS, *i.e.*, to control the solubility of the V_2O_5 (Fig. 3b). In contrast to the pure powders, the vanadate elution from a composite containing V_2O_5 nanowires was lower than from one containing commercial V_2O_5 (Fig. 2b), *i.e.*, the vanadate level after t = 8 days of exposure to the PBS medium was more than four times lower. The 0D sub-micron particles were not observed on the surface of the V_2O_5/PLGA composite after 4 days of exposure to the PBS (Fig. 3b). We observed just 200 nm-sized holes at the PLGA surface, because hydrolytic degradation of the PLGA had begun. Similarly, the formation of up to 1 μm-sized pores was

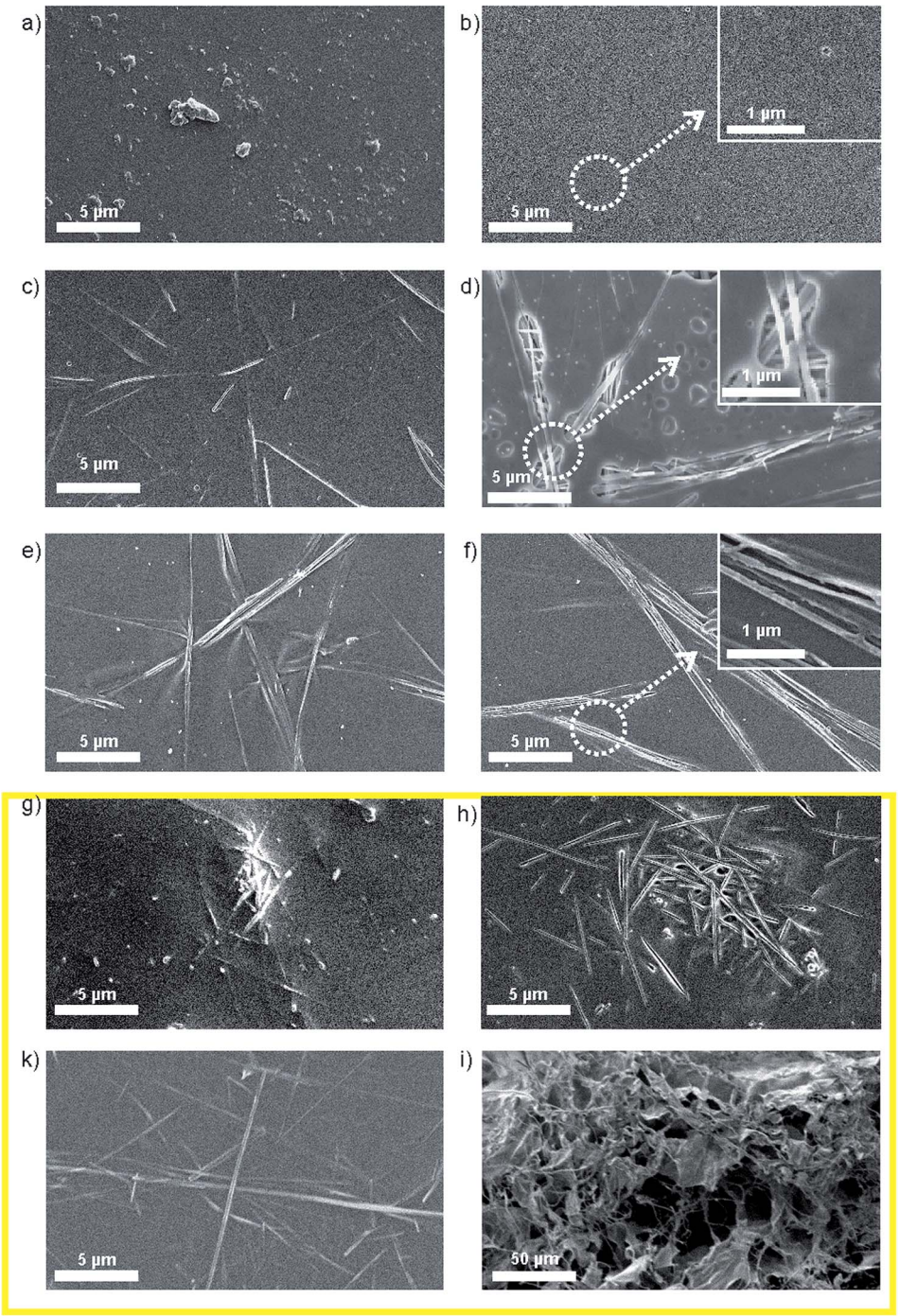

Fig. 3 SEM micrographs of surface of V_2O_5 MPs/PLGA composite (a) before and (b) after exposure to PBS; V_2O_5 NWs/PLGA (c) before and (d) after exposure to PBS; V_2O_5 NWs/PLA (e) before and (f) after exposure to PBS; V_2O_5 NWs/PS (g) before and (h) after exposure to PBS; V_2O_5 NWs/chitosan (k) before and (i) after exposure to PBS.

also observed on the surface of the V_2O_5 nanowires/PLGA composite (Fig. 3d). However, the nanowires were still attached to the surface. They were partly exposed to the PBS medium, as just parts of their length were completely covered by the PLGA.

The SEM study of the V_2O_5/PLGA surface indicated that the 0D sub-micron particles diffuse from the PLGA surface into the PBS, while the diffusion of the nanowires is hindered. As a consequence, the elution of the vanadate ions from the V_2O_5-nanowires/PLGA composite is slower than from the commercial V_2O_5/PLGA composite. In both cases, the coating thickness was not changed after 1 day of exposure to the PBS, *i.e.* the body of the polymer matrix was still stable (Fig. S2b and d†). We concluded that the 1D nanoparticle morphology of the V_2O_5 allows more efficient control of the vanadate elution compared to the 0D sub-micron particle morphology.

Surface of the prepared V_2O_5 NWs/polymer composites

To analyse the ability of different polymers to control the solubility of V_2O_5 nanowires, we incorporated them inside various polymeric carriers. Before the exposure to the PBS medium the surface morphology of the prepared composites was investigated (Fig. 3). The reference composite based on the PLGA matrix exhibited embedded 0D sub-micron V_2O_5 particles on the surface (Fig. 3a). The extent of the V_2O_5 particles' coverage with the polymer matrix varied. Some particles were almost completely covered with the PLGA matrix, while others were just slightly immersed inside the matrix. A similar distribution of V_2O_5 MPs was observed at the surface of V_2O_5 MPs/PLA and V_2O_5 MPs/chitosan composites (Fig. S1a and c†). In comparison to the 0D V_2O_5 MPs, we observed that the coverage of the 1D V_2O_5 NWs by the PLGA matrix was better (Fig. 3c), as just small portions of the individual nanowires were exposed to the environment. The nanowires were dispersed along the matrix and lay almost in plane with the surface. We observed a similar distribution of nanowires at the surface of the V_2O_5 NWs/PLA and V_2O_5 NWs/chitosan (Fig. 3e and k). We observed a similar distribution of nanowires at the surface of the V_2O_5 NWs/PLA and V_2O_5 NWs/chitosan (Fig. 3e and k). In contrast, at the surface of V_2O_5 NWs/PS composites bunches of agglomerated nanowires were identified (Fig. 3g).

The thickness of the analysed composites was between 10 and 15 μm (Fig. S1c, e and g†). They did not contain bubbles as a consequence of solvent evaporation (Fig. S2c, e and g†).

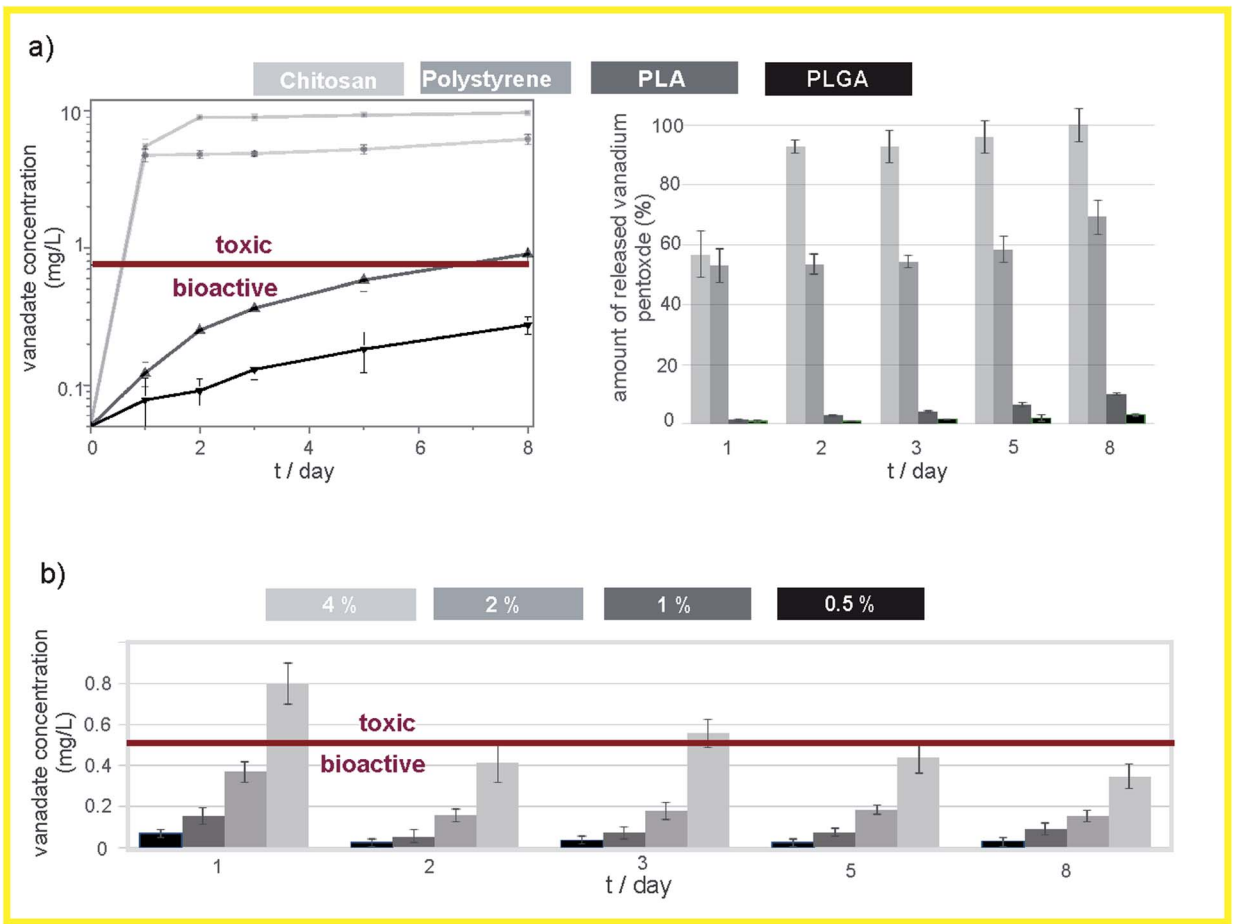

Fig. 4 (a) The cumulative vanadates elution kinetics from different V_2O_5 NWs/polymer composites, presented as either an increase in vanadate concentration in PBS or the percentage of released V_2O_5 from polymer matrix; (b) daily vanadates' elution from PLGA matrix containing 0.5%, 1%, 2% and 4% of V_2O_5 NWs.

Behaviour of the coatings made from different V_2O_5 NWs/polymer composites under *in vitro* conditions.

The release of vanadates from the V_2O_5 NWs/PLGA does not show any significant initial burst effect and the release of vanadates is constant over time (Fig. 4a). The concentration of the released vanadates is within the bioactive concentration range (below the mark, Fig. 4a). Similarly, the elution kinetics of the vanadates from the V_2O_5 NWs/PLA (Fig. 4a) showed no initial burst effect, but the final concentration was no longer within the bioactive concentration range and the amount of the released vanadates after 8 days of exposure to the PBS was almost four times higher when compared to the V_2O_5 NWs/PLGA composite (Fig. 4a). The morphology of the V_2O_5 NWs/PLA surface revealed holes in the shape of the nanowires after 1 day long exposure to the PBS, which implies that the PLA matrix is not efficient for the retention of the nanowires (Fig. 3f). In addition, the PLA matrix was also not able to retain the V_2O_5 MPs (Fig. S1b†). In the case of the V_2O_5/PS composite, almost 55% of the incorporated V_2O_5 was released after 1 day of exposure to the PBS, while in the next 7 days only 10% of the material was released, *i.e.*, the initial burst effect was observed (Fig. 4a). The overall concentration of the vanadates is an order of magnitude above the bioactive range (Fig. 4a). The morphology of the V_2O_5 NWs/PS surface exhibited holes in the shape of the nanowires after the exposure to the PBS, proving the burst release of whole nanowire agglomerates (Fig. 3h). In all three cases (V_2O_5 NWs/PLGA, V_2O_5 NWs/PLA and V_2O_5 NWs/PS) the coating thickness was not changed after 1 day of exposure to the PBS, *i.e.* body of polymer matrix was still stable (Fig. S2d, f and h†).

The V_2O_5 NWs/chitosan composite exhibited the lowest ability to control the elution kinetics of the vanadates. Namely, more than 90% of the incorporated nanowires were dissolved from the V_2O_5 NWs/chitosan composite after 2 days of exposure to the PBS (Fig. 4a). In contrast to the other V_2O_5/polymer systems, the coating collapse was observed in the SEM

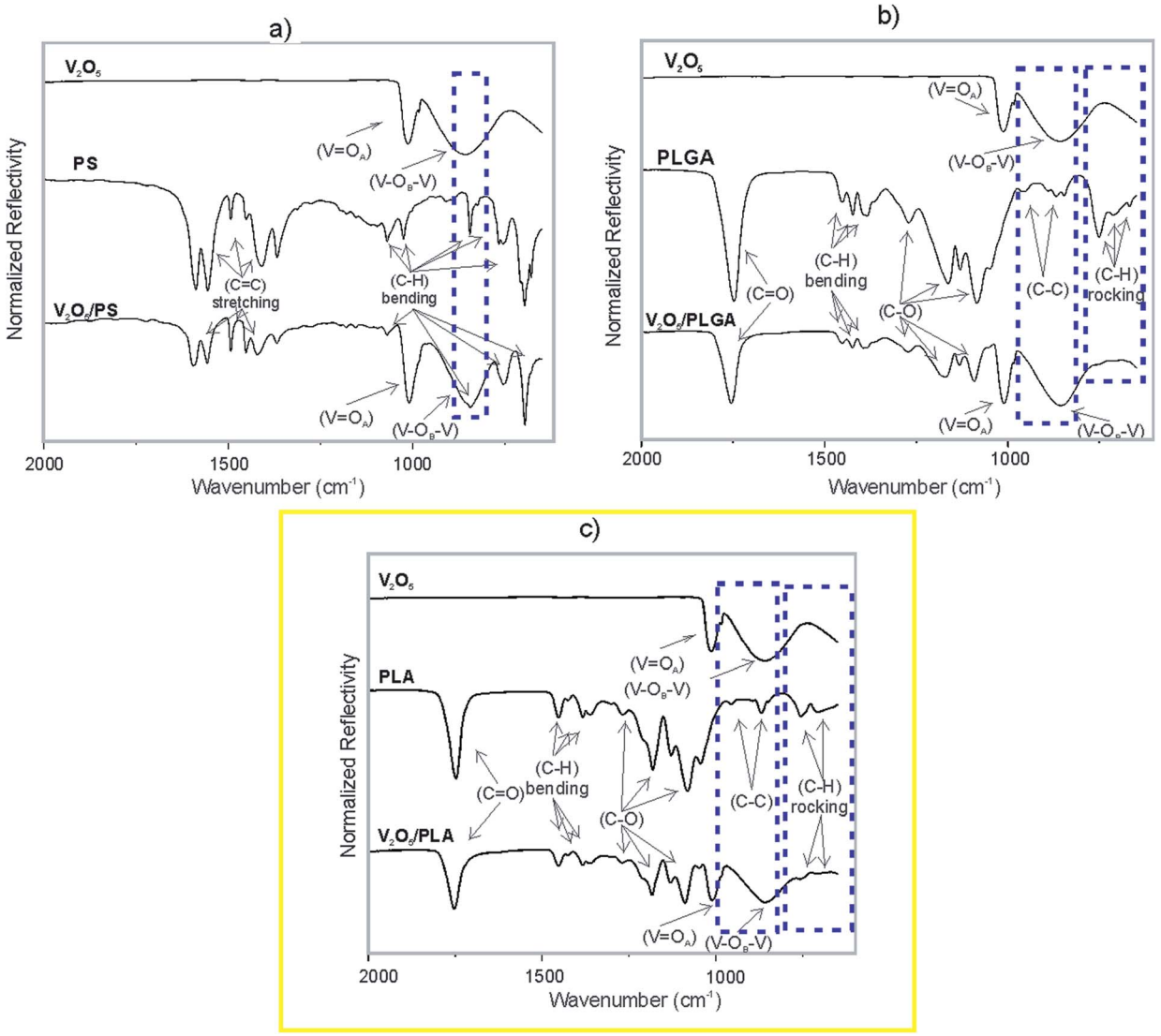

Fig. 5 ATR-IR spectrum of (a) V_2O_5 NWs, PS and V_2O_5 NWs/PS; (b)V_2O_5 NWs, PLGA and V_2O_5 NWs/PLGA; (c) V_2O_5 NWs, PLA and V_2O_5 NWs/PLA.

micrograph of the V_2O_5 NWs/chitosan surface, which could be related to the swelling of the matrix and the up-take of water from the medium (Fig. 3h). As a result, the thickness of the coating increased from 10 μM to more than 200 μM (Fig. S2h†). The collapse of the chitosan matrix was also observed after the exposure of the V_2O_5 the MPs/chitosan to the PBS medium (Fig. S1d†).

The daily elution study of the vanadate release from the V_2O_5 NWs/PLGA composites confirmed the absence of any initial burst effect (Fig. 4c). The maximum allowed amount of embedded V_2O_5 NWs inside the PLGA matrix is 2%, as higher loadings resulted in a vanadate release outside the bioactive concentration range (Fig. 4c).

The study showed that the PLGA, the PLA and the PS differ in their ability to control the dissolution of the nanowires. The polarity of these polymers (based on contact-angle measurements) decreases from PLGA over to PLA to PS,[23–25] same as their ability to control vanadate release from the corresponding V_2O_5 NWs/polymer composites. Therefore, we anticipated that the polarity of the polymer matrix is related to the strength of the interface interactions at the V_2O_5/polymer interface. In contrast, the chitosan is a highly hydrophilic polymer with a high swelling rate, *i.e.*, the ability to absorb a large amount of water.[26] We showed that swelling of the matrix has a negative influence on the control of vanadate elution from the V_2O_5 NWs/chitosan composite due to the coating's collapse. Thus, in the following section dedicated to interphase interactions, the V_2O_5 NWs/chitosan composite was not evaluated.

Study of the interface interactions in the V_2O_5 NWs/polymer composites

The nature of the interphase interactions inside the V_2O_5 NWs/polymer composites was studied by the means of FT-IR technique. The ATR-IR spectrum of the V_2O_5 nanowires (Fig. 5a) consists of two absorption maxima. The sharp one, at 1012 cm^{-1}, is assigned to the vibration modes of the V=O_A bond. This oxygen is bonded to a single vanadium atom. The broad band at 858 cm^{-1} corresponds to the vibrations of the V–O_B–V structure. The O_B is bonded to two vanadium atoms and is a bridging atom between two corner-sharing octahedra.[27,28] The ATR-IR spectrum of PS (Fig. 5a) showed the presence of its characteristic bands. The absorption maxima in the range from 1400 to 1600 cm^{-1} correspond to the C=C stretching vibration of the styrene aromatic rings. The bands in the range from 1000 to 1275 cm^{-1} belong to the in-plane C–H bending, while the absorption maxima in the range from 600 to 900 cm^{-1} belong to the out-of-plane C–H bending.[29] The ATR-FTIR spectrum of the V_2O_5/PS composite is a combination of the individual V_2O_5 and PS IR spectra (Fig. 5a). In the regions where individual bands are overlapping, a convolution of peaks is observed (*e.g.*, the band of PS at 854 cm^{-1} convolutes with the V_2O_5 band at 858 cm^{-1}, as indicated).

The ATR-IR spectrum of the PLGA (Fig. 5b) and PLA (Fig. 5c) showed the presence of characteristic bands of polyesters. The absorption bands at 668, 712 and 753 cm^{-1} correspond to the C–H rocking vibrations.[30,31] The sharp absorption maximum at

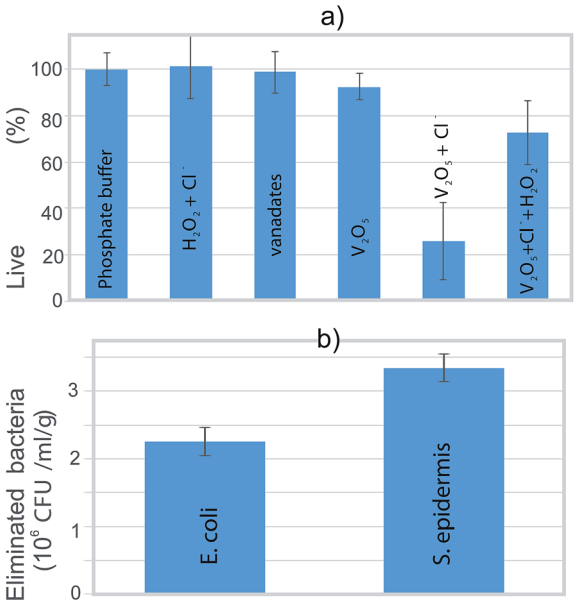

Fig. 6 (a) The percentage of live bacteria after 3 h exposure to various media and (b) the number of eliminated bacteria after exposure to phosphate buffer containing V_2O_5 and chloride ions.

1746 cm^{-1} is assigned to the vibration of the carbonyl group (C=O).[30,31] The bands at 1271, 1162, 1130, 1084 and 1050 cm^{-1} are assigned to the C–O stretching bond vibration, while the bands at 1452, 1432, 1393, 1384 and 1366 belong to the C–H bending vibrations. Furthermore, the absorption maxima at 956, 922, 891, 868 and 846 cm^{-1} correspond to the C–C stretching vibrations.[30,31] Not all of the vibrational modes of the V_2O_5 and the PLGA are present in the IR spectrum of the V_2O_5/PLGA (Fig. 5b). The peaks corresponding to the C–H rocking vibration are not present (indicated by a dashed rectangle). These vibration bands are present in the IR spectra of V_2O_5 NWs/PLA, but are strongly reduced in intensity (Fig. 5c). It is not clear whether the C–C stretching vibration bands are still present in both, the V_2O_5 NWs/PLGA and V_2O_5 NWs/PLA composites as they overlap with the strong V–O_B–V band of the V_2O_5 (indicated by a dashed rectangle).

These results indicate the presence of strong intermolecular interactions at the V_2O_5 NWs/PLGA interface, as the C–H vibration maxima of the PLGA matrix are overwhelmed. These interphase interactions were also observed within the V_2O_5 NWs/PLA composite, but are weaker in intensity than within the V_2O_5 NWs/PLGA, because C–H rocking vibrations were just partially overwhelmed. In contrast, the IR analysis confirmed absence of such interactions within the V_2O_5/PS composite.

Interaction of V_2O_5 nanowires and the V_2O_5/PLGA composite coatings with biological systems

We tested the ability of the V_2O_5 nanowires to eliminate the bacteria *via* the catalysis of the hydrogen-peroxide-to-hypochlorite transformation in the presence of Cl^-. Planktonic bacteria with 100% viability (according to a BacLight live/dead assay) were the starting point (Fig. 6a). This starting

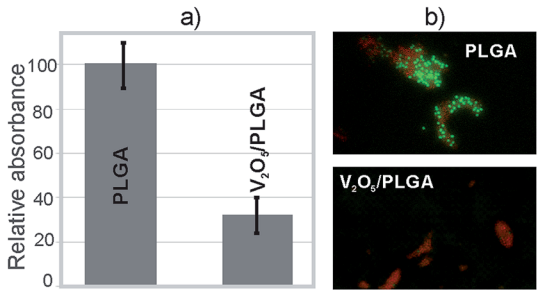

Fig. 7 (a) The relative absorbance at 590 nm of extracted crystal violet solutions and (b) BacLight live/dead imaging of attached *S. epidermidis* at the surface of the coatings. Composites contained 2% of vanadium pentoxide.

viability of the bacteria was not significantly influenced when the vanadates, the V_2O_5 nanowires or a combination of H_2O_2 and Cl^- (without V_2O_5) were added to the phosphate buffer (Fig. 6a). These results indicated that neither the pure form of the V_2O_5 nor the released vanadates were able to harm the bacteria. However, the joint effect of the V_2O_5 and the chloride ions reduced the bacteria's viability by 75%. At the same time, the solution where the production of hypochlorite was expected (combined effect of V_2O_5, Cl^- and H_2O_2) lowered the viability by just 25% (Fig. 6a), due to the increased solubility of the V_2O_5 in the presence of H_2O_2.[20] In the phosphate buffer containing V_2O_5 and Cl^-, the number of eliminated *S. epidermidis* (3.3×10^6 CFU ml^{-1} g^{-1}) is higher than the number of eliminated *E. coli* (2.2×10^6 CFU ml^{-1} g^{-1}). Using this test, we confirmed the ability of the V_2O_5 nanowires to cause the catalytically induced elimination of both the Gram-positive (*S. epidermidis*) and Gram-negative (*E. coli*) bacterial strains (Fig. 6b).

Testing was also performed for the V_2O_5 NWs/PLGA composite coatings, relating to their ability to prevent bacteria colonization at the surface. After an overnight incubation of the agar plates, on which the solution above the evaluated coatings was smeared after vigorous stirring, no colony growth was observed. This indicated the complete colonization of the *S. epidermidis* at the surface of the coatings. However, a difference in the number of adsorbed bacteria was observed. The CV assay showed that the amount of colonized bacteria on the surface of the V_2O_5 NWs/PLGA composite coatings was more than three times lower than at the surface of the PLGA coating (Fig. 7a). The live/dead assay revealed that the majority of the colonized bacteria at the surface of the V_2O_5 NWs/PLGA composite were dead because the red signal was much stronger than the green signal. In contrast, a significant green signal is observed at the surface of the PLGA, which proved the presence of live bacteria at the surface of the PLGA (Fig. 7b).

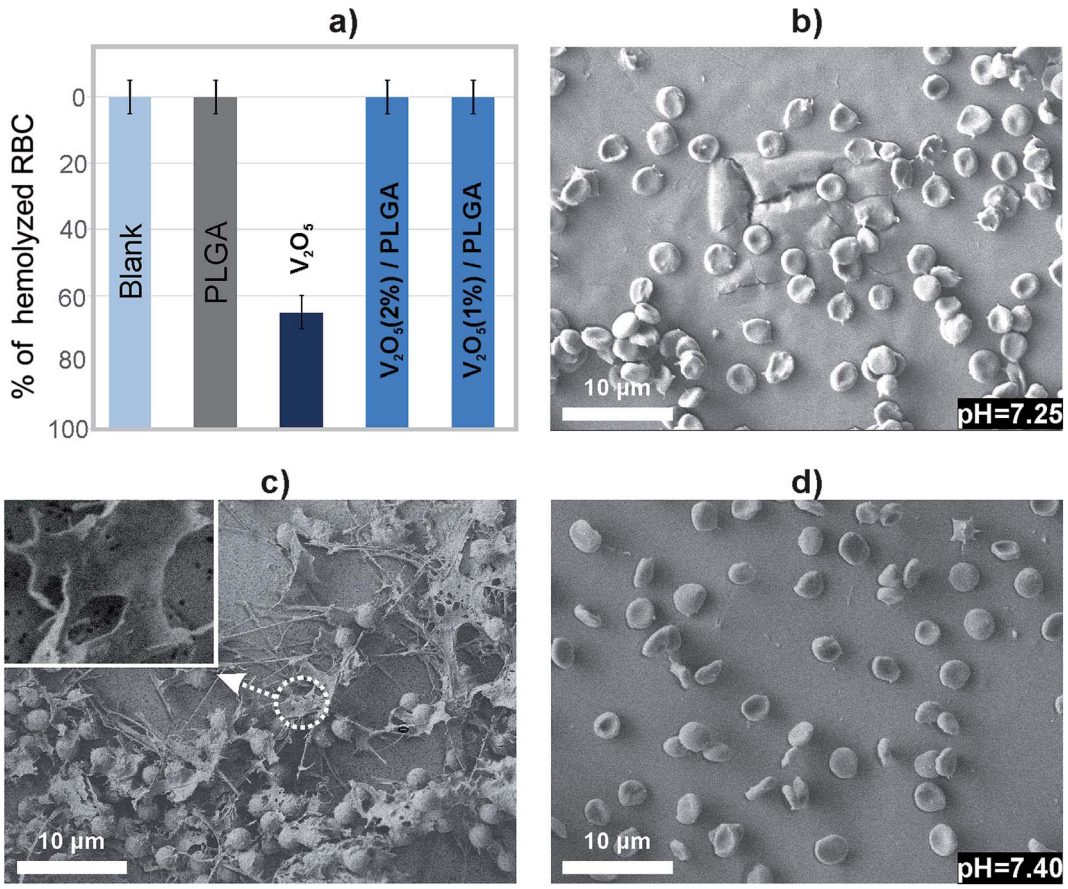

Fig. 8 (a) The percentage of hemolyzed red blood cells after interactions with the prepared materials. SEM morphology of the red blood cells after exposure to the (b) PLGA coating, (c) V_2O_5 nanowires and (d) V_2O_5/PLGA composite coating.

The V_2O_5 nanowires caused hemolysis of 65% of the RBCs, according to the haemoglobin absorption (Fig. 8a). In contrast, the either PLGA or V_2O_5 NWs/PLGA composite coatings showed the absence of hemolysis (Fig. 8a). To evaluate the impact of the RBCs/material interactions on the cell morphology, they were observed by means of the SEM. It was reported that normal RBCs exhibit a smooth biconcave structure.[32] In the case of PLGA coating, the attached RBCs exhibited irregularities in the shape, but there was no membrane rupture observed (Fig. 8b). As the pH of the solution was reduced, we concluded that degradation of PLGA caused a release of the acid products and impacted on the morphology of the RBCs.

The RBCs at the surface of V_2O_5 NWs/PLGA composite coating did not exhibited irregularities at the surface, observed in the case of PLGA as well as membrane-damaged cells (Fig. 8d). There was no drop in the pH of the medium, which indicated the ability of V_2O_5 to modify the degradation of the PLGA.

Discussion

Based on the findings related to the dissolution of free V_2O_5 nanowires and their solubility after embedding in a PLGA matrix, we propose the following mechanism for control over the V_2O_5 dissolution provided by the PLGA matrix (illustrated in Fig. 9).

When exposed to the PBS medium, a single V_2O_5 nanowire interacts with the surrounding water molecules, which causes the introduction of a shear stress at the nanowire due to the large aspect ratio. As a consequence, they are first broken and then dissolved. Even though parts of the individual nanowires in the V_2O_5 NWs/PLGA were exposed (Fig. 3d) to the surrounding water molecules, the stresses induced by the water molecules were transferred along the polymer matrix, resulting in the prevention of the nanowires' breakage and thus their dissolution. However, a small portion of the nanowires diffused out of the matrix and due to the free exposure to water molecules, they eventually dissolved.

Therefore, the success of the V_2O_5 solubility control from the V_2O_5/PLGA depends on hindering the particles' diffusion into the PBS in the early stage of the exposure. V_2O_5 nanowires have a large aspect ratio and are situated almost in-plane with the PLGA surface (Fig. 3c and d). Thus, their diffusion towards the PBS is greatly hindered and a small portion of them are released from the PLGA matrix. This explains the efficient solubility control of the V_2O_5 nanowires inside the PLGA matrix (Fig. 4b). In contrast, the 0D sub-micron particles of the commercial V_2O_5 are randomly oriented inside the PLGA matrix and their diffusion from the matrix is not restricted. This explains why the solubility control of the 0D V_2O_5 in the PLGA matrix is not as efficient as the solubility control of the 1D V_2O_5.

Apart from the PLGA, the PLA, PS and chitosan were also evaluated for their ability to control the solubility of the V_2O_5 NWs. PLGA and PLA are synthetic, biocompatible and biodegradable polymers and are among the best defined polymers for applications in drug delivery.[25] Polystyrene is inert to mammalian cells and is used as a substrate of microplates for testing the cellular response to various stimuli.[33] Chitosan is recognized for its osteoconductive, enhanced wound healing and antibacterial properties, which make it an attractive candidate for use in implant-coating technology.[34]

The strength of the interaction at the V_2O_5 NWs/polymer interface impacts on the diffusion of the V_2O_5 NWs towards the PBS. The PLGA and PLA monomeric units contain polar C–O and C=O bonds. Oxygen is highly electronegative, which induces a positive charge on the neighbouring C atoms. *Via* the inductive effect, this charge is partially transferred to the remaining C and H atoms, causing the creation of a partial positive charge on these atoms (Fig. S3a and b†). As the IR analysis confirmed, the C–H atoms interact with the surfaces of the vanadium pentoxide nanowires where the oxygen atoms are partially negative (Fig. S3a and b†). Thus, we proposed dipole–dipole interface interactions within both the V_2O_5 NWs/PLGA and V_2O_5 NWs/PLA composites (Fig. S3a and b†). The number of C and H atoms is smaller in the PLGA than in the PLA monomeric unit, which causes a higher partial positive charge on the C and H atoms in the PLGA than in the PLA monomeric unit. *i.e.*, the dipole–dipole interactions are stronger within the V_2O_5 NWs/PLGA than within the V_2O_5 NWs/PLA composites (Fig. S3a and b†). Because of that, (i) the C–H vibrations bands are overwhelmed in the IR spectra of the V_2O_5 NWs/PGLA, while greatly reduced (but still present) in the IR spectra of the V_2O_5 NWs/PLA (Fig. 5b and c) and (ii) these interactions are strong enough to retain the nanowires within the PLGA matrix (Fig. 3d), while not sufficient to retain them within the PLA matrix (Fig. 3f). In contrast to the PLA and PLGA, the PS does not contain polar bonds, *i.e.*, there is no charge separation and induction of a partially positive charge (Fig. S3c†). As a consequence, there are no dipole–dipole interphase interactions within the V_2O_5 NWs/PS composites involving C–H bonds and nanowires, which is proved by the absence of any effect on the C–H vibration bands in the IR analysis (Fig. 5a).

Apart from the described influence on the surface morphology of the V_2O_5 NWs/polymer composites after exposure to the PBS and IR spectra, the absence/presence of these interactions plays an important role during the preparation procedure for the composites. In the case of PLGA and PLA, dipole–dipole interphase interactions help stabilize the nanowires in the polymer solution by preventing extensive re-agglomeration (Fig. 3c and e). Without them the nanowires re-agglomerate like in the case of the V_2O_5 NWs/PS (Fig. 3g). As a result, predominantly individual nanowires were released from the PLA surface, while whole bunches of agglomerated nanowires were released from the PS upon exposure to the PBS, making the initial burst effect more pronounced in the case of the PS (Fig. 4a).

The water-swelling properties of the polymer matrix impacted the diffusion of V_2O_5 NWs towards the PBS. It compromised the efficacy of the chitosan to control the release of the vanadates from the V_2O_5 NWs/Chitosan coating.

Regarding the antibacterial potential of V_2O_5 NWs, we related it completely to its ability to catalyse the transformation of hydrogen peroxide to hypochlorite ions. We proposed a two-stage mechanism. Firstly, the V_2O_5 NWs produces a small

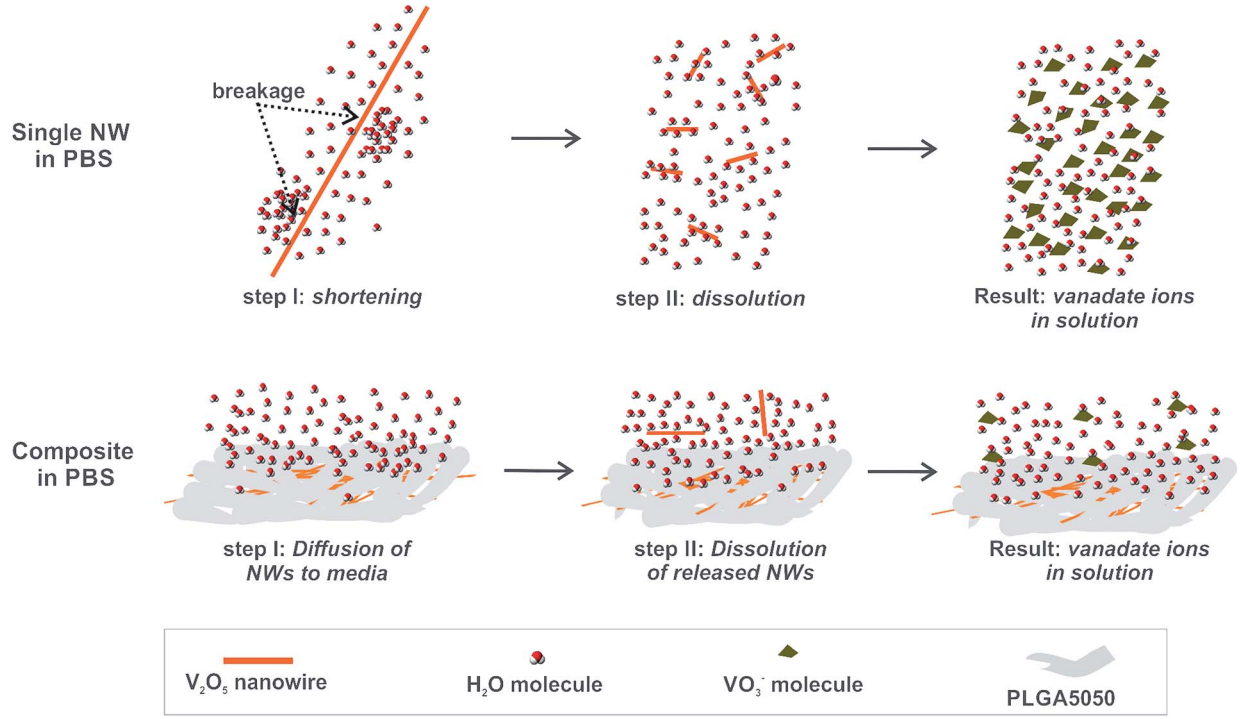

Fig. 9 Proposed mechanism of V_2O_5 solubility control in PLGA matrix.

amount of hydrogen peroxide, as previously suggested.[35] We have confirmed that this amount is not sufficient to affect the bacteria, as their viability was not reduced. However, in the presence of chloride ions, hydrogen peroxide is transformed to hypochlorite ions, which effectively eliminate the bacteria. The further addition of hydrogen peroxide to the solution containing chloride ions reduced the antibacterial potential of the V_2O_5. This was a consequence of the accelerated dissolution of V_2O_5 in the presence of added H_2O_2, which caused the reduced area for catalysis when compared to the V_2O_5 in the phosphate buffer containing chloride ions. Although the ROS production is common for metal oxides,[36] V_2O_5 has a unique ability to transform it to more potent hypochlorite ions.

We exploited the antimicrobial potential of V_2O_5 to protect the PLGA surface. *S. epidermidis* is a representative strain, as it causes more than 30% of all the implant-related bacterial infections.[37] The bacteria concentration used in the evaluations of the V_2O_5 NWs/PLGA antibacterial potential was two orders of magnitude higher than proposed by ISO 22196:2007(E), because the use of lower concentrations led to experiments with large standard deviations. Taking this into account, the V_2O_5 was successful in preventing bacteria adhesion at the surface of the PLGA, as the number of colonized bacteria was 70% lower. The application of the BacLight assay might be problematic for biofilms because the precise number of colonized bacteria was unknown, which might lead to the overexpression of the red colour.[38] Although it was not possible to determine the associated percentages of live and dead bacteria at the surface, we were still able to state, based on the ratios between the red and green colours, that the viability of the attached *S. epidermidis* at the surface of the V_2O_5 NWs/PLGA was reduced when compared to the PLGA surface. Thus, the V_2O_5 exhibited antibacterial protection of the PLGA by both decreasing the number of colonized bacteria and their viability.

When an implant is inserted into the human body, the first cells that come into contact with the device surface are red blood cells.[39] For this reason it is important to evaluate the impact of the surface of the device on the red blood cells. We have proved that the V_2O_5 NWs/PLGA composite coatings neither affected the morphology of the RBCs nor induced their hemolysis.

Conclusions

The newly designed and processed nanowires-V_2O_5/PLGA composite biocoating elutes vanadates within the bioactive concentration range without any initial burst effect, while allowing effective protection against *S. epidermidis* colonization and the absence of any harmful effect on the red blood cells. The underlying mechanism includes strong V_2O_5/polymer interface interactions that hinder the diffusion of V_2O_5 nanowires from the PLGA. The unique ability of V_2O_5 to exhibit self-maintained (no requirement for H_2O_2 in environment) antibacterial activity, based on its myeloperoxidase-like catalytic activity was discovered. These findings highlight the V_2O_5/PLGA composite as an attractive multifunctional material for applications in the technology of implant coating.

Acknowledgements

This research is financed by Slovenian Research Agency grant numbers PR-05560 and P2-0091-0106. We are thankful to Prof. Tadej Malovrh from Institute of Microbiology and Parasitology (VF, UL) for supplying fresh sterile sheep blood and to Martin

Štefanič, PhD for his advices regarding designing tests on red blood cells.

Notes and references

1 G. Subbiahdoss, R. Kuijer, D. W. Grijpma, H. C. van der Mei and H. J. Busscher, *Acta Biomater.*, 2009, **5**, 1399–1404.
2 R. André, F. Natálio, M. Humanes, J. Leppin, K. Heinze, R. Wever, H. C. Schröder, W. E. G. Müller and W. Tremel, *Adv. Funct. Mater.*, 2011, **21**, 501–509.
3 F. Natalio, R. André, A. F. Hartog, B. Stoll, K. P. Jochum, R. Wever and W. Tremel, *Nat. Nanotechnol.*, 2012, **7**, 530–535.
4 B. Amulic, C. Cazalet, G. L. Hayes, K. D. Metzler and A. Zychlinsky, *Annu. Rev. Immunol.*, 2012, **30**, 459–489.
5 S. Ivanković, S. Musić, M. Gotić and N. Ljubesić, *Toxicol. In Vitro*, 2006, **20**, 286–294.
6 K. B. Fischer, PhD thesis, Karlsruhe Institute of Techology, 2009.
7 J. D. Jarrell, B. Dolly and J. R. Morgan, *J. Biomed. Mater. Res., Part A*, 2009, **90**, 272–281.
8 D. A. Barrio, M. D. Braziunas, S. B. Etcheverry and A. M. Cortizo, *J. Trace Elem. Med. Biol.*, 1997, **11**, 110–115.
9 A. M. Cortizo, V. C. Sálice, C. M. Vescina and S. B. Etcheverry, *BioMetals*, 1997, **10**, 127–133.
10 K. E. Moyer, A. A. Saba, R. M. Hauck and H. P. Ehrlich, *Exp. Mol. Pathol.*, 2003, **75**, 80–88.
11 H. P. Ehrlich, K. A. Keefer, G. O. Maish, R. L. Myers and D. R. Mackay, *Plast. Reconstr. Surg.*, 2001, **107**, 471–477.
12 M. Y. Lee and H. P. Ehrlich, *J. Cell. Physiol.*, 2008, **217**, 72–76.
13 D. M. Facchini, V. G. Yuen, M. L. Battell, J. H. McNeill and M. D. Grynpas, *Bone*, 2006, **38**, 368–377.
14 A. Ścibior, H. Zaporowska, A. Wolińska and J. Ostrowski, *Cell Biol. Toxicol.*, 2010, **26**, 509–526.
15 A. Kumari, S. K. Yadav and S. C. Yadav, *Colloids Surf., B*, 2010, **75**, 1–18.
16 W. B. Liechty, D. R. Kryscio, B. V. Slaugther and N. A. Peppas, *Annu. Rev. Chem. Biomol. Eng.*, 2010, **1**, 149–173.
17 H. Palza, *Int. J. Mol. Sci.*, 2015, **16**, 2099–2116.
18 Y. Fu and W. J. Kao, *Expert Opin. Drug Delivery*, 2010, **7**, 429–444.
19 B. S. Kim, J. M. Oh, H. Hyun, K. S. Kim, S. H. Lee, Y. H. Kim, K. Park, H. B. Lee and M. S. Kim, *Mol. Pharm.*, 2009, **6**, 353–365.
20 W. Avansi, C. Ribeiro, E. R. Leite and V. R. Mastelaro, *Cryst. Growth Des.*, 2009, **9**, 3626–3631.
21 X. He, M. Tubino and A. V. Rossi, *Anal. Chim. Acta*, 1999, **389**, 275–280.
22 G. A. O'Toole, *J. Visualized Exp.*, 2011, 3–5.
23 Y. Yuan and T. R. Lee, *Surface Science Techniques*, Springer - Verlag, Heidelberg, 2013, vol. 51.
24 Y. Li, J. Q. Pham, K. P. Johnston and P. F. Green, *Langmuir*, 2007, **23**, 9785–9793.
25 H. K. Makadia and S. J. Siegel, *Polymers*, 2011, **3**, 1377–1397.
26 M. Rinaudo, *Prog. Polym. Sci.*, 2006, **31**, 603–632.
27 L. Abello, E. Husson, Y. Repelin and G. Lucazeau, *Spectrochim. Acta, Part A*, 1983, **39**, 641–651.
28 L. D. Frederickson and D. M. Hausen, *Anal. Chem.*, 1963, **35**, 818–827.
29 B. Stuart, *Infrared Spectroscopy: Fundamentals and Applications*, John Wiley & Sons, Chichester, UK, 1st edn, 2004, vol. 40.
30 M. Jevtic, A. Radulovic, N. Ignjatovic, M. Mitric and D. Uskokovic, *Acta Biomater.*, 2009, **5**, 208–218.
31 R. M. Silverstein, F. X. Webster and D. Kiemle, *Spectrometric Identification of Organic Compounds*, Wiley, Hoboken, 7th edn, 2005.
32 P. V. Asharani, S. Sethu, S. Vadukumpully, S. Zhong, C. T. Lim, M. P. Hande and S. Valiyaveettil, *Adv. Funct. Mater.*, 2010, **20**, 1233–1242.
33 T. G. Van Kooten, H. T. Spijker and H. J. Busscher, *Biomaterials*, 2004, **25**, 1735–1747.
34 J. D. Bumgardner, R. Wiser, P. D. Gerard, P. Bergin, B. Chestnutt, M. Marini, V. Ramsey, S. H. Elder and J. A. Gilbert, *J. Biomater. Sci., Polym. Ed.*, 2003, **14**, 423–438.
35 J. L. Ingram, A. B. Rice, J. Santos, B. Van Houten and J. C. Bonner, *Am. J. Physiol.: Lung Cell. Mol. Physiol.*, 2003, **284**, 774–782.
36 E. Matijevic, in *Fine Particles in Medicine and Pharmacy*, Springer Science, 2011, p. 57.
37 D. Campoccia, L. Montanaro and C. R. Arciola, *Biomaterials*, 2006, **27**, 2331–2339.
38 L. Netuschil and T. Auschill, *BMC Oral Health*, 2014, **14**, 2.
39 Z. Chen, T. Klein, R. Z. Murray, R. Crawford, J. Chang, C. Wu and Y. Xiao, *Mater. Today*, 2016, **19**, 304–321.

